

Bioinspiration & Biomimetics



PAPER

Enhanced detection performance in electrosense through capacitive sensing

RECEIVED
18 May 2016

REVISED
29 June 2016

ACCEPTED FOR PUBLICATION
6 July 2016

PUBLISHED
8 August 2016

Yang Bai¹, Izaak D Neveln², Michael Peshkin¹ and Malcolm A MacIver^{1,2,3,4}

¹ Department of Mechanical Engineering, Northwestern University, Evanston, IL, USA

² Department of Biomedical Engineering, Northwestern University, Evanston, IL, USA

³ Department of Neurobiology, Northwestern University, Evanston, IL, USA

⁴ Author for correspondence.

E-mail: maciver@northwestern.edu

Keywords: artificial electrosense, capacitive sensing, object identification, underwater robotics

Supplementary material for this article is available [online](#)

Abstract

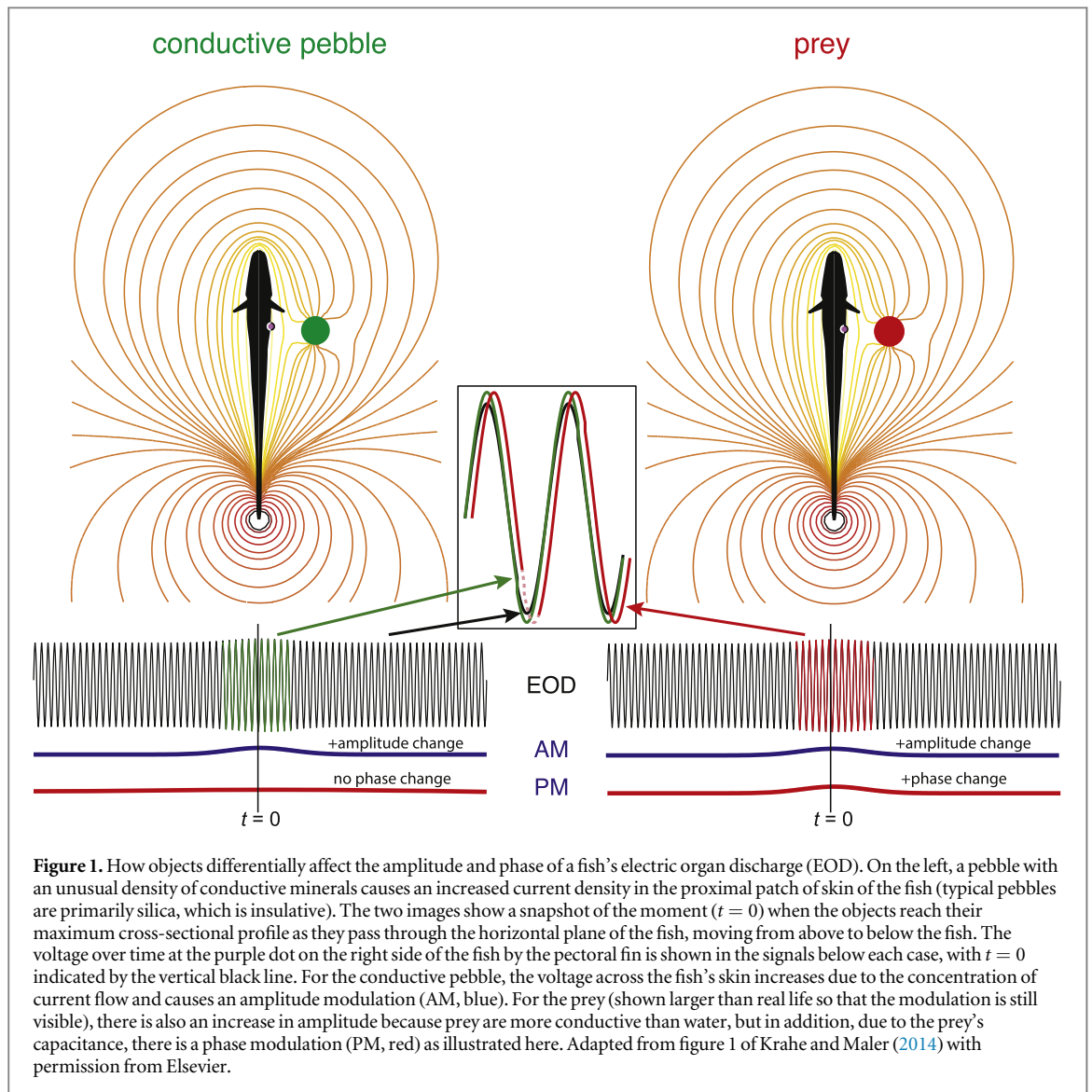
Weakly electric fish emit an AC electric field into the water and use thousands of sensors on the skin to detect field perturbations due to surrounding objects. The fish's active electrosensory system allows them to navigate and hunt, using separate neural pathways and receptors for resistive and capacitive perturbations. We have previously developed a sensing method inspired by the weakly electric fish to detect resistive perturbations and now report on an extension of this system to detect capacitive perturbations as well. In our method, an external object is probed by an AC field over multiple frequencies. We present a quantitative framework that relates the response of a capacitive object at multiple frequencies to the object's composition and internal structure, and we validate this framework with an electrosense robot that implements our capacitive sensing method. We define a metric for comparing the electrosensory range of different underwater electrosense systems. For detecting non-conductive objects, we show that capacitive sensing performs better than resistive sensing by almost an order of magnitude using this measure, while for conductive objects there is a four-fold increase in performance. Capacitive sensing could therefore provide electric fish with extended sensing range for capacitive objects such as prey, and gives artificial electrolocation systems enhanced range for targets that are capacitive.

1. Introduction

Sensory systems transduce the energy of their effective stimulus along multiple dimensions of the stimulus energy. These dimensions are sometimes independently analyzed by parallel processing pathways. For example, auditory stimuli have intensity (amplitude) and phase components that are independently processed by auditory systems (Takahashi *et al* 1984), while movement processing versus color processing of visual stimuli are streamed into different parallel divisions of the visual system (Merigan and Maunsell 1993). In electrosense, certain species of freshwater fish are able to detect nearby objects through the alterations those objects cause to a self-generated electric field (Lissmann and Machin (1958); reviews: Turner *et al* (1999), Krahe and Fortune (2013)). Two key aspects of the alterations objects can cause to a self-

generated field are, first, a change in amplitude of the voltage detected at electroreceptors scattered over the body surface, and second, a change in phase (with respect to the emitted field's phase) at electroreceptors (figure 1). These two aspects are analyzed by two parallel pathways: 'P-type' afferents encode changes in amplitude, while 'T-type' afferents encode changes in phase (Scheich *et al* 1973), with some overlap (Carlson and Kawasaki 2008).

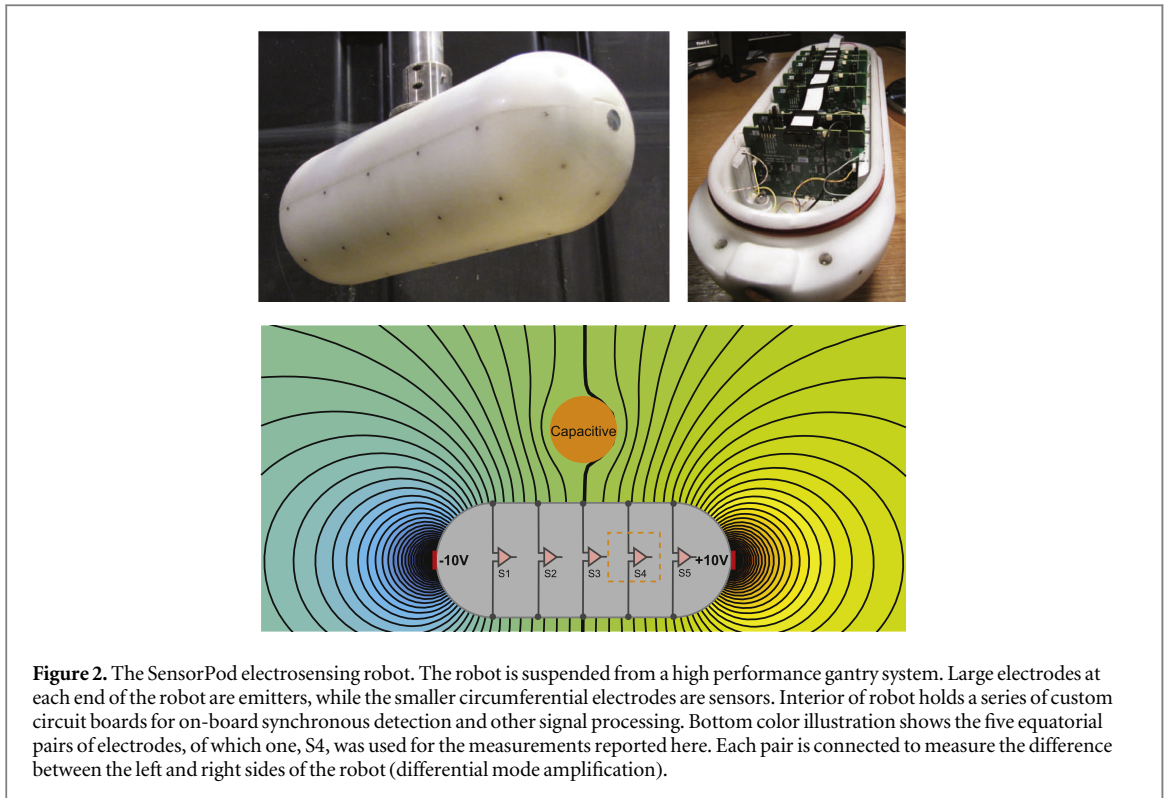
For example, nearby objects that are either less conductive or more conductive than the surrounding water cause large amplitude perturbations, resulting in large changes in voltage at electroreceptors, and large changes in the corresponding P-type sensory afferent's firing rate, while far objects cause small amplitude perturbations and correspondingly smaller changes in firing rate. Objects similarly differ in how much they change the phase of the emitted field. Objects without



capacitance, such as water, or pure conductors or insulators, cause only an amplitude perturbation and not a phase perturbation. However, most living organisms, such as the prey eaten by electric fish, differ in conductivity compared to water but also have capacitance due to the presence of less conductive body exteriors and cellular membranes, and can therefore cause a perturbation in the amplitude and phase at electroreceptors (von der Emde 1990, 1998, Nelson *et al* 2002).

The neural pathways for processing amplitude perturbations have been more extensively characterized than those that process phase perturbations. Similarly, robots implementing electrosense have focused on sensing amplitude perturbations (Solberg *et al* 2008, Boyer *et al* 2012, 2013 Neveln *et al* 2013), although an algorithm based on capacitive electrosense has been proposed (Ammari *et al* 2013, 2014). For this study, we devised a robotic electrosense platform that can measure the phase perturbations caused by capacitive objects. With this system we find that phase perturbation measurements arising from

objects with capacitance have higher signal to noise ratios (SNR), resulting in enhanced detection and localization of capacitive objects (Ammari and Wang 2016). Our results point to the possibility that in the initial stages of prey capture, when targets are furthest away (MacIver *et al* 2001), behavior may be mediated by the phase pathway. Enhanced detection due to the low noise of the phase component of perturbations may help explain why prey can be detected at distances that are beyond what measurements and modeling of the amplitude pathway suggest should be possible with that pathway alone (Maler 2009). Consistent with this hypothesis, a sensory structure called the dorsal filament on the dorsum of weakly electric fish (specifically Gymnotiforms) has been shown to be studded with sensors that have the anatomical features of phase-encoding electroreceptors (Franchina and Hopkins 1996). The dorsum of the body, which has a higher density of electroreceptors than the rest of the trunk (Carr *et al* 1982), has been shown to be important in detection of prey (MacIver *et al* 2001). Furthermore, prior measurements of live prey indicate that



the phase shift they cause to an electric field is maximal at typical field frequencies of electric fish (MacIver 2001, Nelson *et al* 2002).

A useful analogy for the enhanced performance of the phase pathway is to consider how different properties of light are transduced in visual systems (Caputi and Budelli 2006). Sensors that detect only luminance of light generate gray scale images. Adding the ability to detect color (light wavelength) increases the contrast of a colored object in a gray background of similar luminance. Analogously, phase detection in electro-sense should enable a capacitive object to pop out of a background dominated by purely resistive sources, such as the water in which the fish swims. Prey could thereby be detected further away than purely resistive detritus of similar geometry and bulk conductivity.

2. Methods

We know from prior work described above that electric fish are sensitive to both the amplitude and phase of field perturbations caused by objects. These two components of a perturbation clearly exist independently of the biological details of the fish's transduction system. Here we describe our technical approach to measuring these two aspects of voltage perturbations. Our approach does not attempt to mimic the manner in which fish accomplish transduction of amplitude and phase, the biophysical details of which are not well understood.

In our robotic electrosense system (hereafter SensorPod), the voltage perturbation caused by an

external object is measured by sending the signal from a voltage sensor on one side of the body, and a second sensor on the opposite side of the robot (figure 2) to a differential amplifier (Solberg *et al* 2008). The differentially amplified signal is then processed using a synchronous detector circuit (also referred to as a lock-in amplifier) to extract the very small changes that ride on top of the large emitted field.

In synchronous detection, the received signal is multiplied with two reference signals as shown in figure 3. One of the reference signals is identical to the emitted field signal and in phase with it, and the other is 90° out of phase. See Bai *et al* (2015) for additional references on synchronous detection.

Intuitively, the in-phase measurement shown in figure 3 is sensitive to both resistive and capacitive properties of objects, whereas the out of phase measurement is sensitive only to the capacitance of objects arising from non-zero phase shift ϕ . By measuring the relative magnitude of the in-phase and out-of-phase components, we can compute the phase angle ϕ as $\phi = \text{atan}(V_{\text{out-phase}}/V_{\text{in-phase}})$.

2.1. Estimating object capacitance and internal structure

Object capacitance and internal structure are estimated when the objects are stationary relative to the SensorPod underwater. The analytical framework to estimate capacitance and internal structure is derived from the framework established in our previous work (Bai *et al* 2015). Extensions to this framework are presented in the supplementary material. We briefly describe the process here.

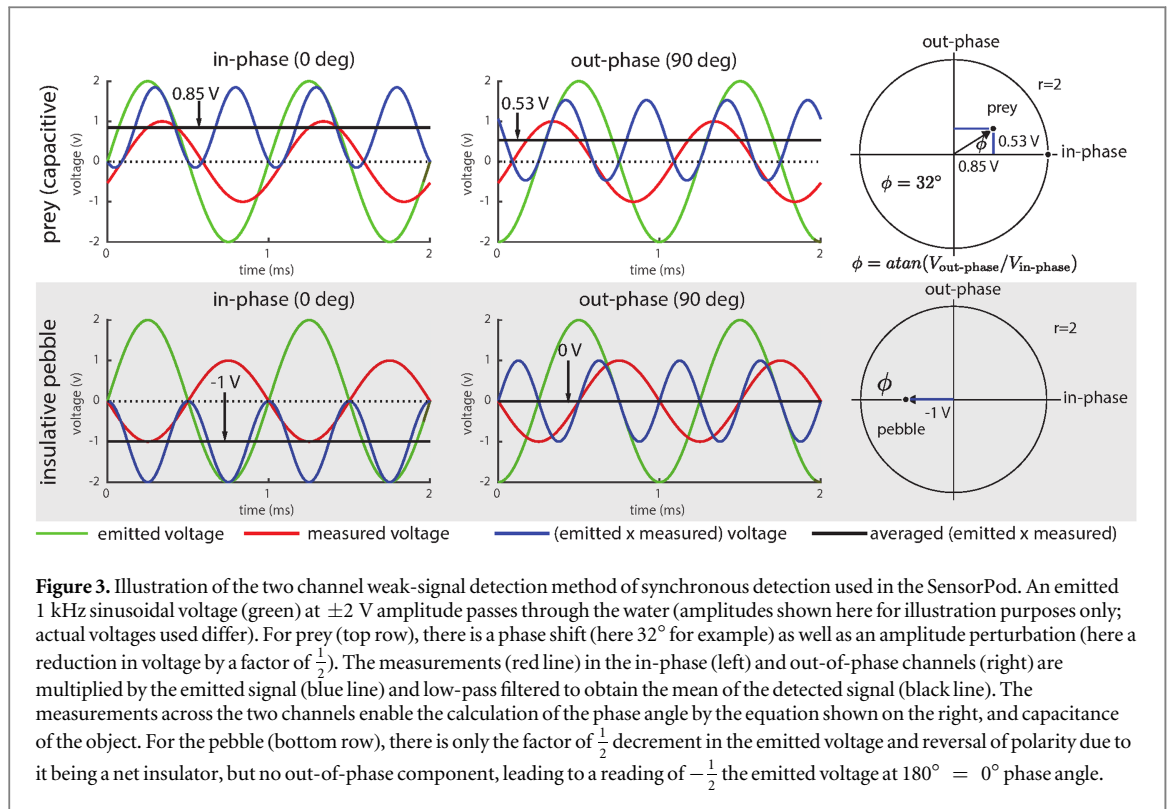


Figure 3. Illustration of the two channel weak-signal detection method of synchronous detection used in the SensorPod. An emitted 1 kHz sinusoidal voltage (green) at ± 2 V amplitude passes through the water (amplitudes shown here for illustration purposes only; actual voltages used differ). For prey (top row), there is a phase shift (here 32° for example) as well as an amplitude perturbation (here a reduction in voltage by a factor of $\frac{1}{2}$). The measurements (red line) in the in-phase (left) and out-of-phase channels (right) are multiplied by the emitted signal (blue line) and low-pass filtered to obtain the mean of the detected signal (black line). The measurements across the two channels enable the calculation of the phase angle by the equation shown on the right, and capacitance of the object. For the pebble (bottom row), there is only the factor of $\frac{1}{2}$ decrement in the emitted voltage and reversal of polarity due to it being a net insulator, but no out-of-phase component, leading to a reading of $-\frac{1}{2}$ the emitted voltage at $180^\circ = 0^\circ$ phase angle.

The capacitance of a sphere with a thin film of layered conductive and dielectric materials can be calculated from object properties by

$$C_{\text{film}} = \epsilon_{\text{rel}} \epsilon_0 \frac{4\pi R^2}{d_{\text{film}}}. \quad (1)$$

ϵ_0 is the vacuum permittivity and is equal to $8.85 \times 10^{-12} \text{ F m}^{-1}$. ϵ_{rel} is the relative permittivity of the dielectric material and is 3.1 for Mylar which was used in this work to create capacitive spheres. R is the sphere radius and d_{film} is the film thickness. C_{film} , which is based solely on object properties, can be compared to estimates of capacitance derived from electro-sensory measurements.

The key for estimation using the SensorPod is to sweep the frequency of the emitted field until the in-phase channel is zero with non-zero out-of-phase reading. Such a response corresponds to a 90° phase shift and a purely imaginary point in the frequency response. We call the corresponding frequency of the emitted field the *critical frequency* f_{crit} and its angular version $\omega_{\text{crit}} = f_{\text{crit}}/2\pi$.

A simple relationship between ω_{crit} and the bulk permittivity of an object, ϵ_{bulk} , can be derived using a first-order frequency response model of a spherical object in a uniform field (see supplementary material for the full derivation):

$$\epsilon_{\text{bulk}} = \frac{\sqrt{2} \sigma_{\text{water}}}{\omega_{\text{crit}}}, \quad (2)$$

where σ_{water} is the water conductivity. By determining ω_{crit} from electro-sensory data, we use equation (2) to determine ϵ_{bulk} of the whole sphere. Assuming a

sphere made of homogeneous dielectric material, we can express its capacitance as

$$C_{\text{obj}} = \epsilon_{\text{bulk}} \frac{4\pi R^2}{2R} = \epsilon_{\text{objrel}} \epsilon_0 2\pi R. \quad (3)$$

The size of an object can also be estimated from electro-sensory data (Bai *et al* 2015). We then compare C_{obj} estimated from electro-sensory measurements to the thin film capacitance C_{film} calculated from equation (1).

More complex objects may have multiple layers of different dielectric materials warranting a deeper analysis of the full frequency response. With this additional complexity, the response increases in order (i.e. the number of poles and zeros increases with each layer), adding additional features to the frequency response as detailed in supplementary material.

2.2. Analysis of electro-sense performance

Active electro-sensory system performance can be assessed with respect to two fundamental tasks: object detection and estimation of an object's position. We first define a metric called electro-sense sensitivity to quantify the ability to detect objects. We then also provide statistical measures to quantify the quality of position estimation.

2.2.1. Detection

Sensitivity is the smallest change in signal that a measurement system can detect. This change in the signal must overcome baseline noise levels that are present in the absence of objects. Here, we investigate the ability of our artificial electro-sense device to detect

the presence of an external object. Intuitively, the smaller and further away an object, the harder it is to detect. In this work, for an object of a certain size, we experimentally determine the maximum distance that yields a detectable signal. We can also estimate the smallest object that could be detected at a fixed distance using scaling relationships between the voltage perturbation and the size, composition, and distance of the object. We use SensorPod's excitation electrode separation (approx. 46 cm) as the fixed distance because it determines the electric field configuration. Thus, we can define electrosense sensitivity as either the detection range of certain sized objects or the smallest detectable object volume given a fixed distance.

In our experiments, we move the SensorPod at a fixed velocity in a straight line by a stationary object while continually collecting measurements. Such a set of voltage measurements is called a fly-by profile. To determine electrosense sensitivity, we first establish a detection threshold using statistical analysis between object-present and object-absent fly-by profiles. In order to incorporate the sequential time domain information, we calculate the cumulative sum of the voltage perturbations associated with each fly-by profile and examine the distributions of these sums. We call a distribution from an object-present fly-by a signal distribution and a distribution from an object-absent fly-by a noise distribution.

We treat detection as a binary classification task given the cumulative sum distribution of measurements. Due to noise and drift in measurements (see section 4.5), the voltage measurements are stochastic. We examine the Jensen–Shannon Divergence (JSD) (Lin 1991) between the signal and noise distributions. JSD is a value between 0 and 1 that indicates the similarity between two distributions, with a smaller value associated with higher similarity. We obtain an average noise distribution by averaging the noise distributions from all object-absent fly-by profiles. Having obtained the average noise distribution, we are able to assess detection by comparing the JSD between measurement and noise to a set threshold in JSD value. If the JSD is above the threshold, the object is considered detected.

As is standard for binary classifiers, the choice of threshold (and in this case a JSD value) affects classification performance. We calculate the JSD between individual signal distributions and the average noise distribution. In order to account for the difference in distance, we examined the measurement voltage (V) fall-off with distance (d). Because of the nonlinearity of the electric field, V is related to d as the following

$$V \propto d^{f(d)}, \quad (4)$$

where $f(d)$ is a negatively valued function. Simulation results show $f(d)$ is roughly constant at -4 but does vary slightly with distance, consistent with prior measurements and analyzes (Rasnow 1996, Nelson

and MacIver 2006). In this paper, we scale detection distance to the standard distance (electrode separation) following $V \propto d^{-4}$.

Equation (4) also presents a convenient way to scale measurement object distance to a fixed distance of 46 cm as the following

$$V \propto \text{volume} \propto d^{-4}. \quad (5)$$

To summarize, we quantify sensitivity as the maximum distance of a sphere of fixed size whose fly-by profile (signal distribution) has a JSD (compared to the object-absent noise distribution) above a threshold. Then, using scaling functions, we determine the minimum size sphere detectable at a fixed distance. The data and specific choice of JSD value will be covered in the results.

2.2.2. Position estimation

While detection concerns a sensor's classification ability (object present or not), position estimation concerns the sensor's ability to measure a continuous variable. Good performance in this context corresponds to a narrow distribution of estimates, across multiple trials, around the true position of the object. We quantify the quality of our position estimation through the extraction of zero-crossings across multiple fly-bys of a spherical object. A zero-crossing is where the voltage reading transits between positive and negative, and in ideal conditions should occur when the spherical object center crosses the line connecting the two electrodes of the sensing pair, in which both electrodes would measure the same voltage due to the symmetry of the field (Bai *et al* 2015).

However, it is possible that a fly-by profile has multiple zero-crossings due to noise. Across ten trials at one object distance, we combine all the zero-crossings from every trial fly-by profile and calculate the median and interquartile range to quantify both the accuracy (proximity of the median to the true location) and precision (narrowness of interquartile range) of our estimate.

2.3. Experiment

2.3.1. Apparatus

The experimental platform is the same as described in our previous work (Bai *et al* 2015). We used two basic experimental setups: one for 'dry-dock' experiments in which water was simulated with discrete components and underwater experiments.

For the dry-dock experiments, the SensorPod was taken out of water and connected to a network of resistor elements in series and parallel meant to model water. To model an object embedded within this approximation of water, we used a resistor-capacitor combination that replaced a single resistor at the desired object location. Dry-dock experiments are a simple proof-of-concept showing the efficacy of our system for measuring complex perturbations that include amplitude and phase distortions. The dry-

dock experiments also allow for characterization of other effects not included in our models, such as the parasitic capacitance discussed in the supplementary material.

The underwater setup has the SensorPod submerged underwater with objects nearby. Three types of test objects are used. (1) Insulating PVC pylons (11 cm diameter, 0.6 cm shell, 60 cm length) were used to calibrate the electronics' frequency-dependent, circuit-induced gain attenuation and phase shifts. For more information and results of experiments with these objects, see supplementary information. (2) Capacitive objects were created by wrapping metalized Mylar foil (Mylar side out) over rubber spheres. Metalized Mylar films of different thicknesses and rubber spheres of different sizes are used to obtain different capacitance values. These capacitive objects were attached to a wooden rod with the bottom of the Mylar sealed by a zip-tie and hot glue to prevent electrical current leaking through water. These objects were used to verify that the detected phase shift is indeed caused by the capacitance of objects rather than artifacts in the electronics or the underwater environment. The capacitance values (C_{obj}) estimated using the critical frequency and bulk material equivalence (see supplementary material) are compared against capacitance values (C_{film}) calculated as thin film using equation (1). (3) Three natural capacitive objects, tomatoes of two varieties and three sizes, were measured to demonstrate the ability to detect and identify their internal structures. The tomatoes were placed in water with varying conductivities, see table 2 in supplementary material.

2.3.2. Fly-by experiments to assess detection and estimation performance

We designed experiments in order to compare sensory readings from an environment with an external object to those without an external object. We collected fly-by profiles for pairs of identical trajectories with and without the object present. We used three objects of the same size but different electrical properties: capacitive, insulative, and conductive. The capacitive object was one of the rubber spheres wrapped in metalized Mylar as described above. The insulative object was the unwrapped rubber sphere and the conductive object was a metal sphere. We first selected the emitted field frequency that yields the maximum response in the out-of-phase channel for the capacitive object (not to be confused with the critical frequency described earlier). Then experiments are carried out for each object, with fly-bys that proceed along a linear path in the same plane as the object at lateral distances ranging from 30 to 90 cm. For each scenario (with and without object) and distance configuration, ten fly-by trials (with identical SensorPod trajectories) were collected. These data were used to assess detection and longitudinal position estimation quality as described above.

Table 1. Capacitance comparison.

Item	Obj 1	Obj 2	Obj 3	Obj 4
Thickness (μm)	6	12	12	6
Diameter (cm)	3	3	2.5	2.5
C_{film} (nF)	26.9	13.5	9.3	18.7
Equi. Rel.	4.17	1.86	1.67	3.16
Permittivity	$\times 10^4$	$\times 10^4$	$\times 10^4$	$\times 10^4$
C_{obj} (nF)	88.4	39.4	29.5	55.9

3. Results

3.1. Estimating capacitance and internal structure

Table 1 shows the C_{obj} , the estimated capacitance based on the measure critical frequencies of four capacitive objects (the rubber spheres wrapped in metalized Mylar foil of varying thickness). These estimated capacitances are compared to the capacitances calculated using the thin film equation (equation (1)). Note that while the magnitudes of the two estimates differ by a factor of about three, that factor is consistent across the various objects.

By analyzing the full frequency response of a target object, we can model the internal structure of objects. For results and discussion on internal structure estimation, please refer to the supplementary material.

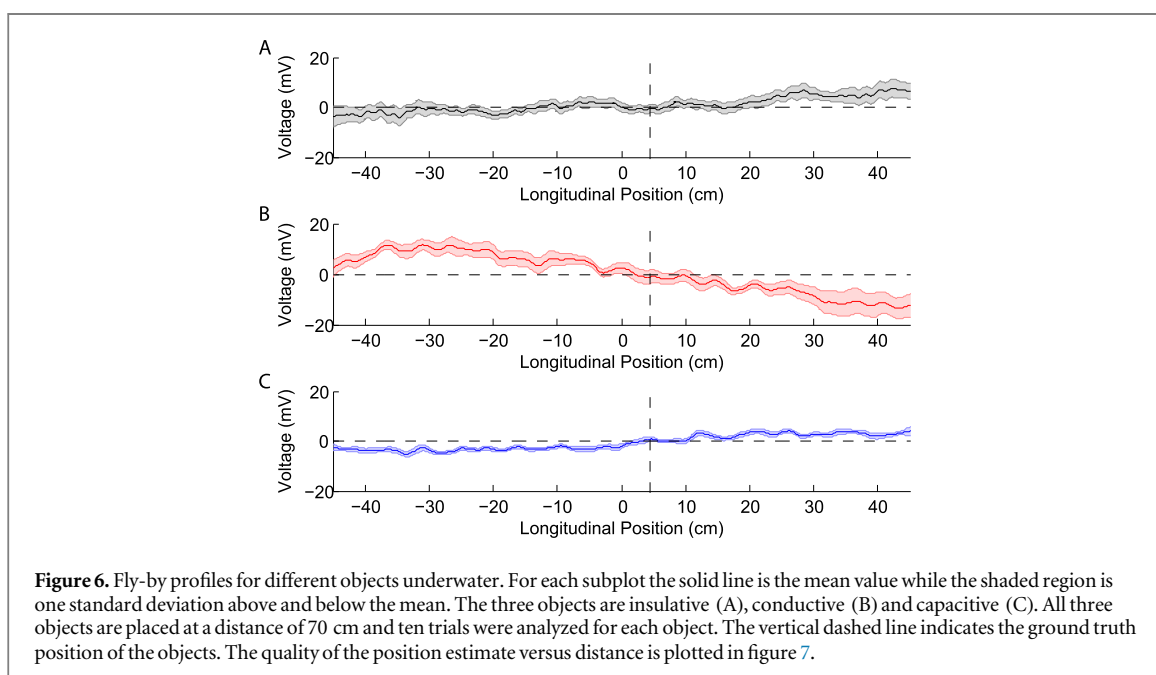
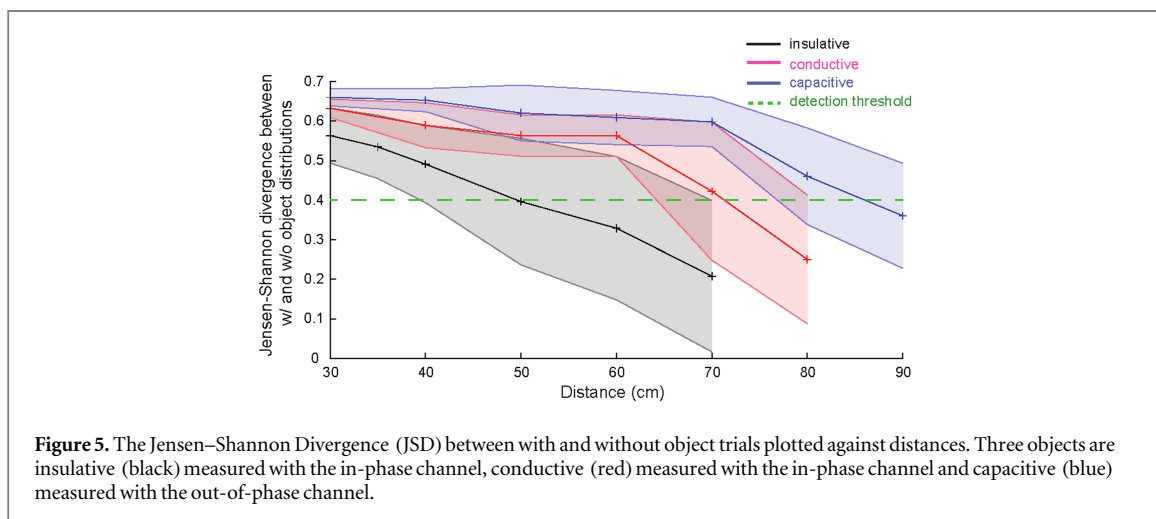
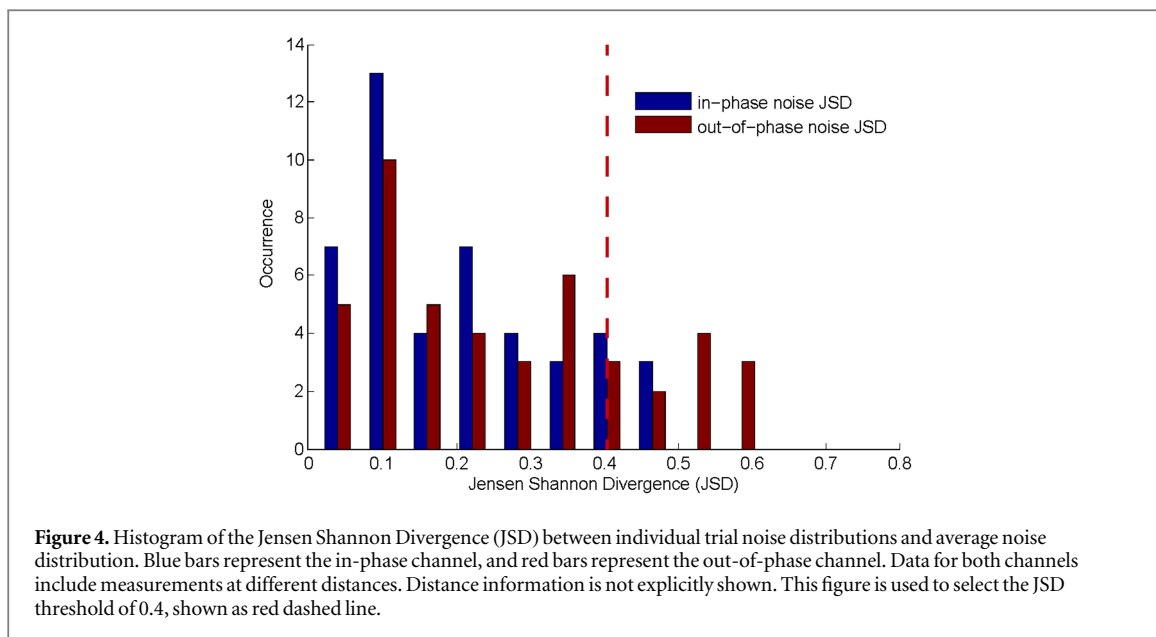
3.2. Electro-sensory performance

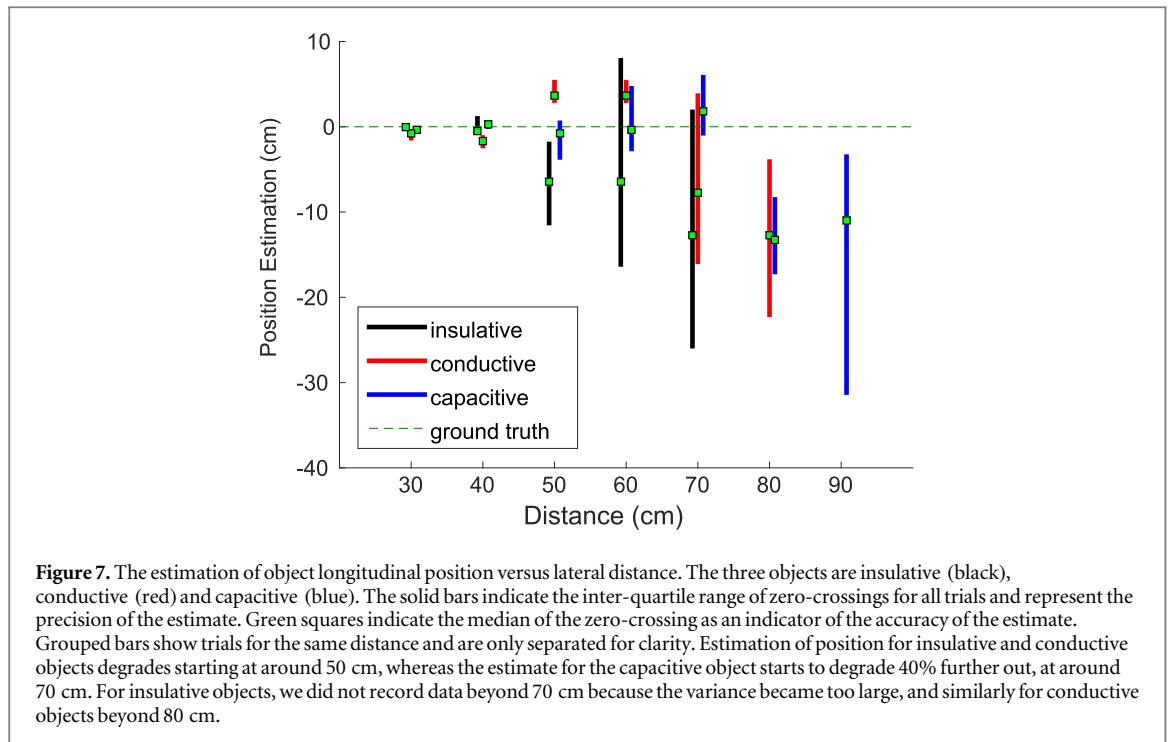
Here we show the results of the performance of capacitive sensing in detection and localization.

3.2.1. Object detection

Figure 4 shows the JSD between individual noise distributions and the averaged noise distribution for both in-phase and out-of-phase channels. Most of individual noise trials have JSD (w.r.t. the averaged noise distribution) less than 0.4 for both resistive and capacitive channels. We select 0.4 as the JSD threshold for determining detection.

In order to determine detection range, we plot the JSD between individual signal distributions and average noise distribution for different object and distance configurations in figure 5. Despite the high variance in JSD, we are able to estimate the electro-sense sensitivity based on the mean values of JSD. In figure 5, the green dashed line representing detection threshold ($\text{JSD} = 0.4$) intercepts three curves at approximately 49 cm for the insulative object, 72 cm for the conductive object, and 86 cm for the capacitive object. Discounting object composition and using equation (5), this translates to electro-sense sensitivity of 180 cm^3 (sphere of radius 3.5 cm) for the insulative object at 46 cm distance, 80 cm^3 (sphere of radius 2.7 cm) for the conductive object at 46 cm distance, and 20 cm^3 (sphere of radius 1.7 cm) for the capacitive object at 46 cm distance. Thus, by this measure, capacitive sensing is better than resistive sensing by nearly an order of magnitude for





insulative objects, and by a factor of four over resistive sensing of conductive objects.

3.2.2. Object position estimation

Figure 6 illustrates the fly-by profiles of three objects at 70 cm. In each subplot, the mean and standard deviation of measurements are plotted as a solid line and shaded regions. The position estimation for a trial is the average of all zero-crossing positions for a fly-by profile. We also show the accuracy of estimation by plotting the inter-quartile range and median of the estimates over many trials as a function of object distance in figure 7. A lower inter-quartile range along with a median close to ground truth indicates higher precision and accuracy and therefore better performance. The estimate of the longitudinal position of the non-capacitive objects starts to degrade at a lateral distance of around 50 cm while the estimate for the capacitive object only starts to degrade around 70 cm.

4. Discussion

By extending our artificial electrosensory system to be sensitive to phase perturbations caused by capacitive objects, we have shown that SNR for detecting and localizing capacitive objects can be higher than for non-capacitive objects. While the current biological literature has extensively discussed a variety of roles for phase perception in electric fish (Heiligenberg 1974, 1975, Matsubara and Heiligenberg 1978, Heiligenberg 1980, Bastian and Yuthas 1984), to our knowledge this is the first time that a gain in distance of object detection has been proposed as an advantage of capacitive sensing. The extended distance range of

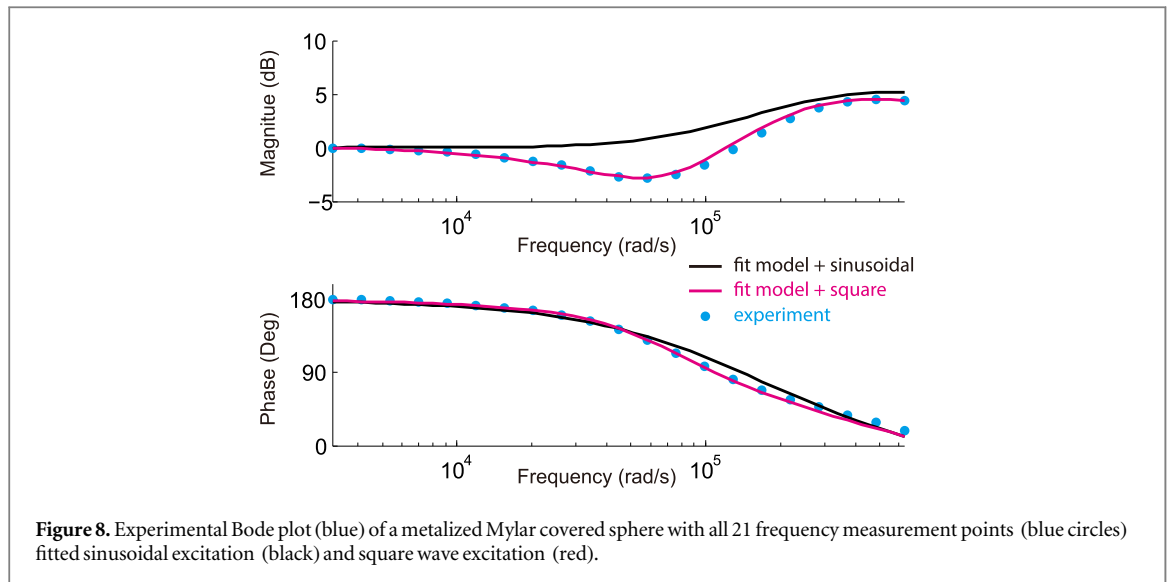
capacitive electrolocation may underlie the gap between theoretical electrolocation distances estimated from amplitude encoders and measured detection distance to live prey (MacIver *et al* 2001, Maler 2009).

4.1. High sensitivity in capacitive sensing

As shown in figure 6, the out-of-phase sensing channel gives lower measurement noise. For capacitive objects, the background effect, mostly from the tank walls and water environment, is eliminated through out-of-phase demodulation. The capacitive channel allows the SensorPod to exclusively sense isolated capacitive objects. Such inherent lower noise floor is reflected in object detection and position estimation. From figures 5 and 7, we observe that the out-of-phase channel has extended range in detection and better accuracy in position estimation compared to the in-phase sensing channel. Comparing figures 5 and 7, we can observe that the distance at which objects reach our detection criterion of $JSD > 0.4$ is larger than the distance at which objects can be accurately localized. For example, insulative objects are at detection threshold at 50 cm in figure 5, whereas at this distance, localization accuracy is significantly degraded according to figure 7. It is intuitive that detection is an easier task than estimation and can be achieved at greater distances.

4.2. Water conductivity adaptation in weakly electric fish

Weakly electric fish work in habitats of widely varying conductivity, from tens of microsiemens per centimeter to three hundred or more microsiemens



(discussion and references in MacIver *et al* 2001, p 552). Such a wide range in habitat conductivity will lead to non-negligible phase shift for prey due to their capacitance. This has been shown in behavioral experiments with fish (von der Emde 1993), and can be appreciated from the prey (top row) case of figure 3, and equation (10) of the supplement. Thus, rather than monitoring a unique phase shift associated with a certain type of prey, such as *Daphnia* with its real and capacitive electrical aspects (Nelson *et al* 2002), the electric fish may need to be able to detect and distinguish a wide range of phase shifts. Without some mechanism of disambiguation, other living organisms that the electric fish do not prey on may look like their prey in terms of phase angle at different water conductivities.

In contrast, water conductivity has no influence on the electric image of insulative objects such as rocks, so the in-phase channel of the fish experiences negligible change. Therefore, for a mixed scene of background rocks with a foreground prey, as water conductivity changes there will be negligible change in the in-phase channel, and significant change in the out of phase channel. The fish will sense this with its T-units, which detect the time difference between its own discharge and the received field.

One hypothesis that could be tested is that the fish accommodates changes in phase angle due to seasonal variation in conductivity simply through associating sensed water conductivities with different desired target phase shifts (time delays).

4.3. The SensorPod can estimate the permittivity and capacitance of objects

We first show the validity and accuracy of using the uniform field analytical models (equations 10 and 17 in supplementary material) in permittivity estimation. Figure 1 in supplementary material shows good agreement between Bode plots from the analytical

models and FEM simulation. For the homogeneous object, the critical frequency method (equation (3)) accurately estimates the relative permittivity to be 30 000. For the shell structure object, the permittivity estimated with our critical frequency method (which assumes one homogeneous material) is 82 000. The effective permittivity (real part of ϵ_{mix} in equation 17 in supplementary material is frequency dependent, and the value is 38 000 at ω_{crit} . The discrepancy is due to that fact that the inside medium conductivity is on par with the water and an in-depth analysis is included in the supplementary material.

Second, we show experimentally that the detected capacitance is indeed caused by the object rather than artifacts like the object holder or the water-electrode interface. For metalized Mylar covered rubber spheres, we compare the calculated capacitance with capacitance derived from experiments. In table 1, the capacitance estimated with critical frequency method (equation (3)) maintains a relatively constant proportion, around 3, to the capacitance computed with equation (1). Another perspective is to look at the Bode plots, as shown in supplementary material figures 7 and 8. The critical frequency point shifts towards lower frequency with higher capacitance (blue and red) and shifts towards higher frequency with higher conductivity of water (red and green). It is important to note that capacitance itself is an inherent property of the object, independent of water conductivity.

Third, we are able to increase the permittivity estimation accuracy of our critical frequency method (equation (3)) by including harmonics from square wave excitation and employing more measurement points. In figure 8, we fit the experimental Bode plot of a metalized Mylar covered sphere with homogeneous sphere analytical model with added harmonics. The relative permittivity from model fitting is 2.24×10^4 , smaller than 3.16×10^4 from critical frequency

Table 2. Sources of noise.

Scenario	High frequency (μV)	Low frequency (μV)
Dry-dock	3.1	10.2
Gantry Off	6.1	18.6
Gantry On	58.6	25.5

method. The discrepancy between the two values is due to the shifted phase plot and therefore shifted critical frequency. Note that such discrepancy is systematic across all capacitive objects. Therefore, for the purpose of comparison among capacitive objects, equation (3) provides a convenient solution.

Lastly, we want to point out some interesting properties of the thin shell model. A thin dielectric shell looks like an object with much higher permittivity (supplementary material equation 17). This fact explains why the small relative permittivity of Mylar (~ 3) yields an equivalent bulk relative permittivity on the order of 10 000. It also provides insight into why living animals, such as the water insects that many electric fish hunt, have high capacitance, as their cell membranes provide many shells.

4.4. Noise and non-ideal effects

Noise in the system stems from three sources. The circuit has inherent noise from the electrical components. A dry-dock experiment was performed by passing electrical signals from the SensorPod through a resistor network and measuring the voltage across one resistor. The gantry motor adds high frequency noise when turned on. The most unpredictable source of noise is from the electrochemistry at the electrode water interface. This source of noise appears mostly as drift, long-term variation in voltage measurements. The electrochemistry induced noise is indirectly obtained by subtracting circuit noise from total noise measured when the gantry motors are turned off. The noise in table 2 is root mean square noise.

Limited tank space is a major non-ideal effect that registers as non-zero reading at the sensor pair without the presence of an external object. This non-zero reading varies from sensor to sensor and also highly depends on the pose of the SensorPod in the tank. The in-phase sensing channel is highly sensitive to the effects of the tank walls, while the out-of-phase channel is insensitive to the same effects. In order to eliminate the effect from the tank walls, we measure the readings solely due to the tank and subtract them from experimental results.

Other non-ideal effects include gain degradation and stray capacitance. These effects attenuate the magnitude by less than 10% at 100 KHz, the highest frequency used. Both subjects are discussed in detail in supplementary material.

5. Conclusion

Our work extends artificial electrosense object identification from conductive and insulative objects to capacitive objects. By probing capacitive objects at multiple frequencies, a quantitative framework enables decoding basic attributes of an object's composition and internal structure. We find that capacitive sensing has significantly higher performance than resistive sensing, nearly an order of magnitude higher range with respect to resistive sensing of insulative objects. We explored several implications for our biological model system, the weakly electric fish, including the sensitivity of capacitive sensing to habitat conductivity, which varies seasonally over a wide range in the rivers where these fish are found.

Acknowledgments

The authors would like to thank HDT Robotics who collaborated in the design of SensorPod and built it as well as the robotic positioning system used in this study. The work is funded by NSF PECASE IOB-0846032, Office of Naval Research Small Business Technology Transfer grant N00014-09-M-0306, with partial support from NSF CMMI-0941674.

References

- Ammari H, Boulrier T and Garnier J 2013 Modeling active electrolocation in weakly electric fish *SIAM J. Sci.* **6** 285–321
- Ammari H, Boulrier T, Garnier J and Wang H 2014 Shape recognition and classification in electro-sensing *Proc. Natl Acad. Sci.* **111** 11652–7
- Ammari H and Wang H 2016 Time-domain multiscale shape identification in electro-sensing *Imaging, Multi-scale and High Contrast Partial Differential Equations 4th Seoul ICM Satellite Conf. on Imaging, Multi-scale and High Contrast PDEs* (Daejeon, Korea, 07–09 August 2014) ed H Ammari et al (American Mathematical society) **66** 23–44
- Bai Y, Snyder J B, Peshkin M and MacIver M A 2015 Finding and identifying simple objects underwater with active electrosense *Int. J. Robot. Res.* **34** 1255–77
- Bastian J and Yuthas J 1984 The jamming avoidance response of *Eigenmannia*: properties of a diencephalic link between sensory processing and motor output *J. Comparative Physiol.* **A 154** 895–908
- Boyer F, Gossiaux P B, Jawad B, Lebastard V and Porez M 2012 Model for a sensor inspired by electric fish *IEEE Trans. Robot.* **28** 492–505
- Boyer F, Lebastard V, Chevallereau C and Servagent N 2013 Underwater reflex navigation in confined environment based on electric sense *IEEE Trans. Robot.* **29** 945–56
- Caputi A and Budelli R 2006 Peripheral electrosensory imaging by weakly electric fish *J. Comparative Physiol.* **A 192** 587–600
- Carlson B A and Kawasaki M 2008 From stimulus estimation to combination sensitivity: encoding and processing of amplitude and timing information in parallel, convergent sensory pathways *J. Comput. Neurosci.* **25** 1–24
- Carr C E, Maler L and Sas E 1982 Peripheral organization and central projections of the electrosensory nerves in gymnotiform fish *J. Comparative Neurol.* **211** 139–53
- Franchina C R and Hopkins C D 1996 The dorsal filament of the weakly electric Apterodontidae Gymnotiformes: Teleostei is specialized for electroreception *Brain Behav. Evol.* **47** 165–78

- Heiligenberg W 1974 Electrolocation and jamming avoidance in a *Hypopygus* (Rhamphichthyidae, Gymnotoidei) an electric fish with pulse-type discharges *J. Comparative Physiol.* **91** 223–40
- Heiligenberg W 1975 Electrolocation and jamming avoidance in the electric fish *Gymnarchus niloticus* (Gymnarchidae, Mormyriiformes) *J. Comparative Physiol.* **103** 55–67
- Heiligenberg W 1980 The jamming avoidance response in the weakly electric fish *Eigenmannia* *Naturwissenschaften* **67** 499–507
- Krahe R and Fortune E S 2013 Electric fishes: neural systems, behaviour and evolution *J. Exp. Biol.* **216** 2363–4
- Krahe R and Maler L 2014 Neural maps in the electrosensory system of weakly electric fish *Curr. Opin. Neurobiol.* **24** 13–21
- Lin J 1991 Divergence measures based on the Shannon Entropy *IEEE Trans. Inf. Theory* **37** 145–51
- Lissmann H W and Machin K E 1958 The mechanism of object location in *Gymnarchus niloticus* and similar fish *J. Exp. Biol.* **35** 451–86
- MacIver M A 2001 The computational neuroethology of weakly electric fish: body modeling, motion analysis, and sensory estimation *PhD dissertation* University of Illinois at Urbana-Champaign UMI, Ann Arbor MI
- MacIver M A, Sharabash N M and Nelson M E 2001 Prey-capture behavior in gymnotid electric fish: Motion analysis and effects of water conductivity *J. Exp. Biol.* **204** 543–57
- Maler L 2009 Receptive field organization across multiple electrosensory maps. II. Computational analysis of the effects of receptive field size on prey localization *J. Comparative Neurol.* **516** 394–422
- Matsubara J and Heiligenberg W 1978 How well do electric fish electrolocate under jamming *J. Comparative Physiol.* **125** 285–90
- Merigan W H and Maunsell J H 1993 How parallel are the primate visual pathways? *Annu. Rev. Neurosci.* **16** 369–402
- Nelson M E and MacIver M A 2006 Sensory acquisition in active sensing systems *J. Comparative Physiol. A* **192** 573–86
- Nelson M E, MacIver M A and Coombs S 2002 Modeling electrosensory and mechanosensory images during the predatory behavior of weakly electric fish *Brain Behav. Evol.* **59** 199–210
- Neveln I D, Bai Y, Snyder J B, Solberg J R, Curet O M, Lynch K M and MacIver M A 2013 Biomimetic and bio-inspired robotics in electric fish research *J. Exp. Biol.* **216** 2501–14
- Rasnow B 1996 The effects of simple objects on the electric field of *Apteronotus* *J. Comparative Physiol. A* **178** 397–411
- Scheich H, Bullock T H and Hamstra R H 1973 Coding properties of two classes of afferent nerve fibers: high-frequency electroreceptors in the electric fish, *Eigenmannia* *J. Neurophysiol.* **36** 39–60
- Solberg J R, Lynch K M and MacIver M A 2008 Active electrolocation for underwater target localization *Int. J. Robot. Res.* **27** 529–48
- Takahashi T, Moiseff A and Konishi M 1984 Time and intensity cues are processed independently in the auditory system of the owl *J. Neurosci.* **4** 1781–6
- Turner R W, Maler L and Burrows M 1999 Special issue on electroreception and electrocommunication *J. Exp. Biol.* **202** 1167–458
- von der Emde G 1990 Discrimination of objects through electrolocation in the weakly electric fish, *Gnathonemus petersii* *J. Comparative Physiol. A* **167** 413–22
- von der Emde G 1993 The sensing of electrical capacitances by weakly electric Mormyrid fish: effects of water conductivity *J. Exp. Biol.* **181** 157–73
- von der Emde G 1998 Capacitance detection in the wave-type electric fish *Eigenmannia* during active electrolocation *J. Comparative Physiol. A* **182** 217–24